Thermal Stability and Crystallization Kinetics of Isotactic Polypropylene/Organomontmorillonite Nanocomposites

Ji-Dong He,[1] Man Ken Cheung,[1] Ming-Shu Yang,[2] Zongneng Qi[2]

[1]*Department of Applied Biology & Chemical Technology, Hong Kong Polytechnic University, Hung Hom, Kowloon, Hong Kong, China*
[2]*State Key Laboratory of Engineering Plastics, Institute of Chemistry, Chinese Academy of Sciences, Beijing, China*

Received 29 April 2002; accepted 6 December 2002

ABSTRACT: The thermal stability and crystallization kinetics of isotactic polypropylene (iPP) and iPP/organomontmorillonite (organo-MMT) nanocomposites were investigated with differential scanning calorimetry and thermogravimetry. The incorporation of organo-MMT up to a concentration of 4 wt % did not affect the melting temperature of iPP but did increase the peak thermal degradation temperature by 60°C. The isothermal crystallization kinetics showed that the addition of organo-MMT increased the crystallization rate of iPP but reduced the isothermal Avrami exponent. The crystallization temperature of the nanocomposites measured with nonisothermal crystallization was higher than that of plain iPP, and this indicated an enhanced crystallization rate. The nonisothermal Avrami exponent, like the isothermal exponent, decreased with the addition of organo-MMT, and this suggested changes in the crystallite growth geometry. Subsequently, the tensile yield strength and the tensile modulus both increased, but the elongation at break and the notched Izod impact strength did not change significantly. © 2003 Wiley Periodicals, Inc. J Appl Polym Sci 89: 3404–3415, 2003

Key words: crystallization; differential scanning calorimetry (DSC); thermogravimetric analysis (TGA); poly(propylene) (PP); nanocomposites

INTRODUCTION

Polymer composites have widely been used in electronics, transportation, construction, and consumer products. They offer unusual combinations of stiffness and toughness that are difficult to attain from individual components. Nanocomposites are defined by the particle size of the dispersed phase having at least one dimension smaller than 100 nm.[1] Nanocomposites possess physical and mechanical properties superior to those of conventional composites based on micrometer-sized fillers.

Polymer/clay nanocomposites are usually synthesized via either intercalation *in situ* polymerization or melt intercalation.[2–9] Melt intercalation may easily be adopted by industry to fabricate polymer/clay nanocomposites with organosilicates and conventional twin-screw compounding extruders.

The layer structure of montmorillonite (MMT) consists of two silica tetrahedral sheets attached to an edge-shared octahedral sheet of either aluminum or magnesium hydroxide. Stacking of the layers (ca. 1 nm thick) by a weak dipolar force leads to interlayers that are occupied by cations such as K^+, Na^+, Ca^{2+}, and Mg^{2+}, through which organosilicates are easily formed by alkylammonium ion-exchange reactions. The organosilicates are broken down into nanoscale building blocks and are dispersed in the polymer matrix to form exfoliated nanocomposites during compounding.[10–13] This article reports the effect of organomontmorillonite (organo-MMT) fillers on the thermal stability and crystallization kinetics of an isotactic polypropylene (iPP) matrix.

EXPERIMENTAL

Preparation of the materials

Samples containing organo-MMT (obtained from Beijing Institute of Chemistry, Chinese Academy of Sciences, Beijing, China) in concentrations of 1, 2, and 4 wt % were prepared by the mixing of adequate amounts of plain iPP (H 1500, Shanghai Chemical Co., China) and then were extruded with a 30-mm twin-screw extruder.[14] The barrel-length/diameter ratio was 27. The extrusion temperatures were set at 150 (zone 1), 220 (zones 2 and 3), and 225°C (die). The rotational speed of the twin screws was 200 rpm. The mechanical properties of plain iPP and iPP/organo-MMT nanocomposites are shown in Table I.

Correspondence to: M. K. Cheung (bckcheung@polyu.edu.hk).

Contract grant sponsor: Hong Kong Research Grant Council; contract grant number: 5299/01P.

TABLE I
Mechanical Properties of Plain iPP and iPP/Organo-MMT nanocomposites

	Plain iPP	1 wt % organo-MMT	2 wt % organo-MMT	4 wt % organo-MMT
Tensile yield strength (MPa)	31.9	35.6	35.0	37.6
Breaking elongation (%)	930.6	846.0	887.1	708.1
Tensile modulus (MPa)	1300	1545	1573	1774
Notched Izod impact strength (kJ/m^2)	3.38	2.70	2.90	3.25

Each tensile specimen had a width of 3.0 mm and a thickness of 3.0 mm. The tensile pulling speed was 50 mm/min. The Izod impact specimens had a dimension of 4 mm × 13 mm × 63 mm. The reported values were averaged from three or five measurements.

Measurement and equipment

Thermogravimetry (TG) analyses were carried out with a PerkinElmer TG7 analyzer. The samples (ca. 10 mg) were measured at a heating rate of 10°C/min under a nitrogen flow (45 mL/min). TG and derivative thermogravimetry (DTG) curves were recorded over the course of heating from room temperature to 800°C.

The melting temperature (T_m) and crystallization kinetics of various polypropylene nanocomposites were studied with differential scanning calorimetry (DSC; Mettler Toledo Stare System). The samples were scanned at a constant heating rate under a nitrogen atmosphere.

Scanning electron microscopy (SEM; Leica) was used to examine the morphology of the cut surfaces of pellets. SEM samples were sputter-coated with 10-nm-thick gold. The SEM micrographs were taken at 20 kV, and the working distance was 9 mm.

RESULTS AND DISCUSSION

Thermal stability

Figure 1 illustrates the DSC curves of plain iPP and nanocomposites containing 1, 2, and 4 wt % organo-MMT at a heating rate of 10°C/min. Figure 1 shows

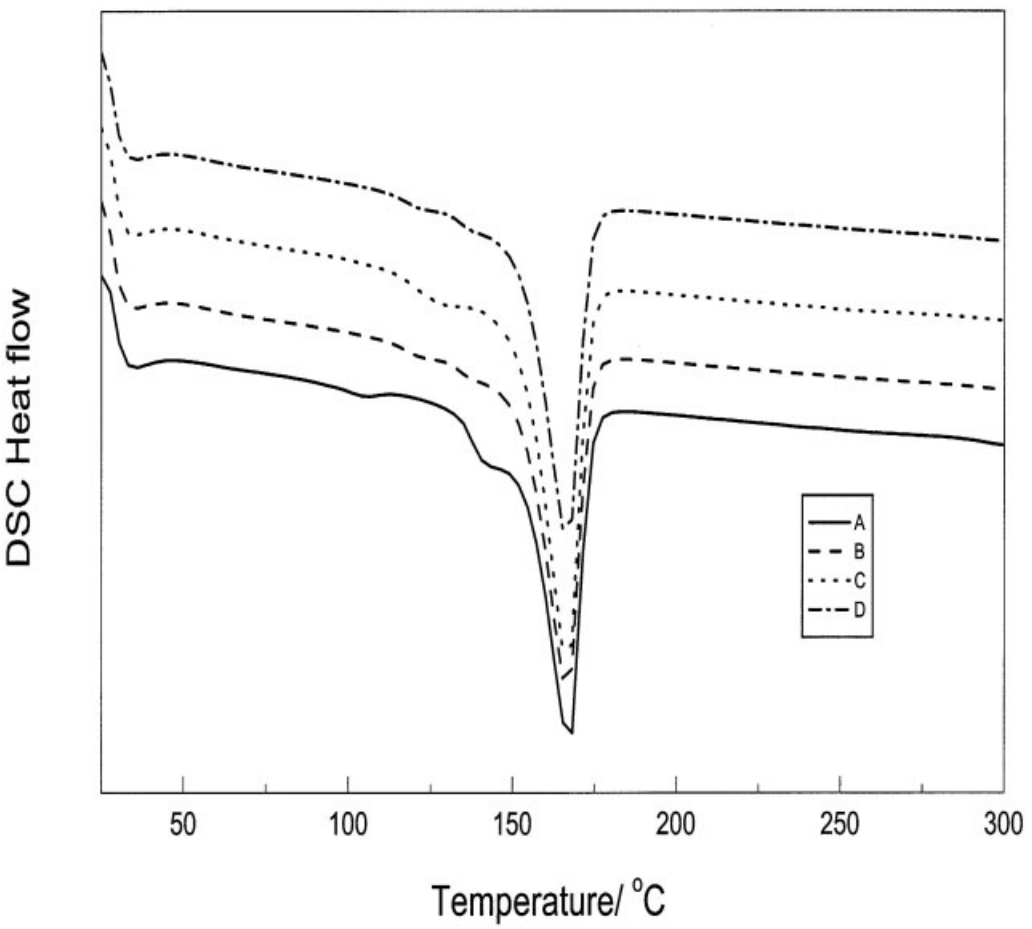

Figure 1 DSC curves of plain iPP and iPP/organo-MMT nanocomposites at a heating rate of 10°C/min: (A) plain, (B) 1 wt % organo-MMT, (C) 2 wt % organo-MMT, and (D) 4 wt % organo-MMT.

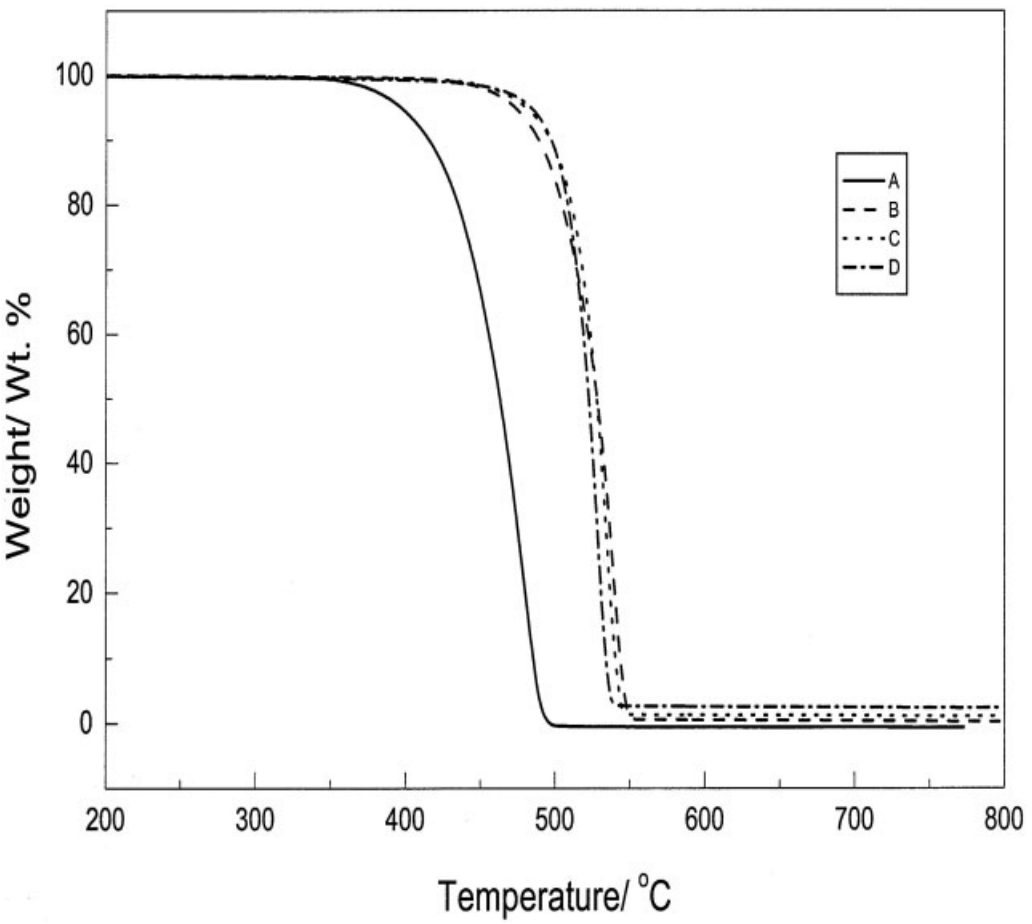

Figure 2 TG curves of plain iPP and nanocomposites: (A) plain, (B) 1 wt % organo-MMT, (C) 2 wt % organo-MMT, and (D) 4 wt % organo-MMT.

that the T_m values of the four samples are nearly the same (ca. 167°C). Figures 2 and 3 show the TG and DTG curves from the thermal degradation of plain iPP and nanocomposites containing 1, 2, and 4 wt % at a heating rate of 40°C/min. The TG curve is a smooth weight-loss curve. The DTG curve shows only one rate-of-weight-loss (dw/dt) peak. This indicates that the degradation consists of one weight-loss step. The incorporation of organo-MMT into the iPP matrix makes the TG and DTG curves shift toward the high-temperature zone. The degradation behavior of the four samples is similar. Table II lists the thermal degradation temperatures of plain iPP and iPP/organo-MMT nanocomposites. T_0 is the temperature at the onset of weight loss. T_p is the temperature at the maximum rate of weight loss, the tip of the DTG curve peak, and T_f is the temperature of complete degradation. T_0 and T_f were obtained from the TG curve with a bitangent method. It is obvious from the figure and table that the incorporation of organo-MMT improves the thermal stability of iPP.

Isothermal crystallization kinetics

For the isothermal crystallization process, the Avrami equation[15] has widely been used to analyze the isothermal crystallization kinetics of polymers:

$$1 - X(t) = \exp(-kt^{n'}) \tag{1}$$

where t is the time, k is the crystallization kinetic rate constant, n' is the isothermal Avrami exponent, and $X(t)$ is the relative crystallization degree. Equation (1) can be linearized as follows:

$$\log[-\mathrm{Ln}(1 - X(t))] = \log k + n' \log t \tag{2}$$

The curves of the heat of fusion versus time for plain iPP and iPP/organo-MMT nanocomposites isothermally crystallized at 130°C from the melt are shown in Figure 4. The Avrami plots of $\log\{-\ln[1 - X(t)]\}$ versus $\log t$ are shown in Figure 5.

All the plots are straight lines at low crystallinities. From the intercepts on the vertical axis at $\log t = 0$ and the slopes, $\log k$ and n' are obtained, respectively.

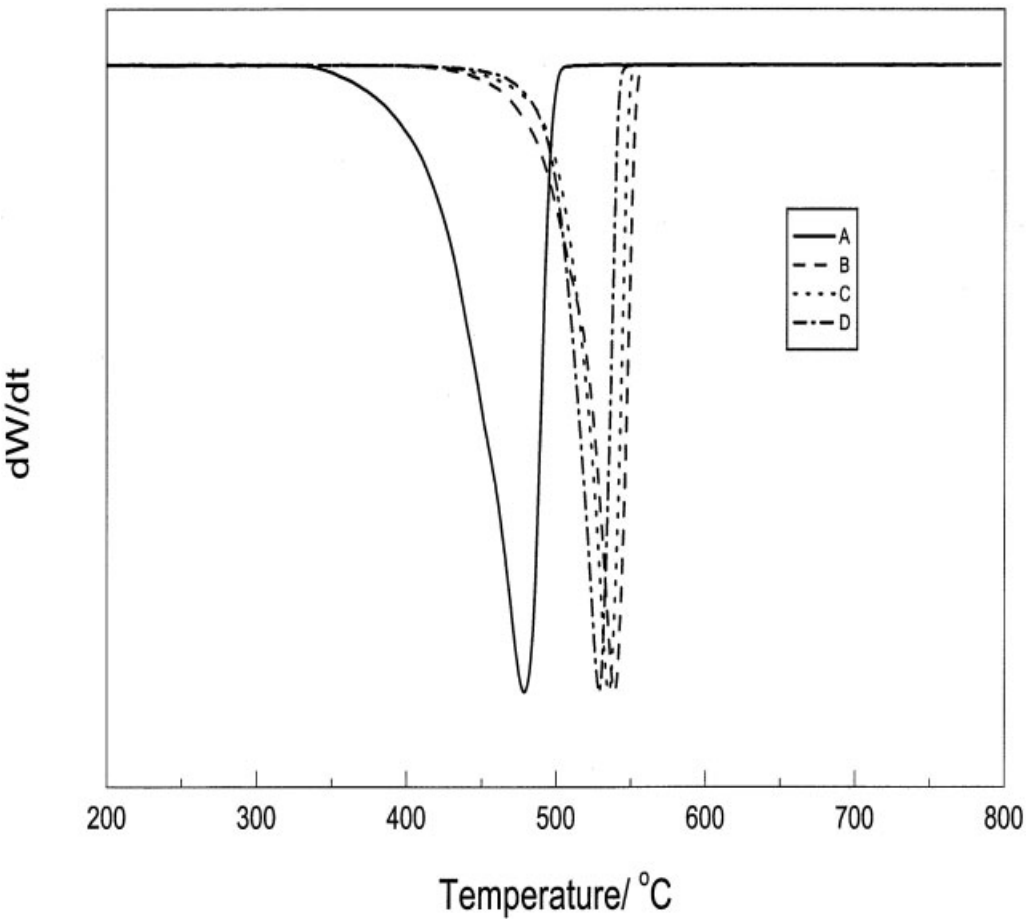

Figure 3 DTG curves of plain iPP and nanocomposites: (A) plain, (B) 1 wt % organo-MMT, (C) 2 wt % organo-MMT, and (D) 4 wt % organo-MMT.

These parameters are listed in Table III. The half-crystallization time ($t_{1/2}$) decreases with the incorporation of organo-MMT into iPP, or the crystallization rate ($1/t_{1/2}$) increases with the weight fraction of organo-MMT. $t_{1/2}$ is obtained as follows:

$$t_{1/2} = (\ln 2/k)^{1/n'} \tag{3}$$

From this crystallization process, n' is determined to be between 2 and 3. Nucleation from polymer composite melts is generally heterogeneous, and n' is not an integer. The Avrami exponent n' increases with the growth dimension, that is, $1 \leq n' \leq 2$ for rodlike growth (one-dimensional), $2 \leq n' \leq 3$ for disclike growth (two-dimensional), and $3 \leq n' \leq 4$ for spherulitic growth (three-dimensional).[16–24]

TABLE II
Thermal Degradation Temperatures of Plain iPP and iPP/Organo-MMT Nanocomposites at a Heating Rate of 40° C/min

	Plain iPP	1 wt % organo-MMT	2 wt % organo-MMT	4 wt % organo-MMT
T_0 (°C)	422.7	502.7	509.8	499.5
T_p (°C)	478.9	540.2	536.4	530.2
T_f (°C)	500.3	556.3	547.6	542.3

Nonisothermal crystallization kinetics

Several models have been proposed for the theoretical treatment of isothermal crystallization kinetics.[25–27] Conversely, only a few models have been developed to explain nonisothermal crystallization, the most important ones being those of Jeziorny,[28] Ziabicki,[29] and Ozawa.[30] In this work, the Ozawa equation is adopted to describe the effect of organo-MMT on the nonisothermal crystallization of iPP at a constant cooling rate. Ozawa extended the Avrami equation, originally for isothermal crystallization, to the nonisothermal case by assuming that the sample is cooled at a constant rate and that the mathematical analysis proposed by Evans[26] is appropriate. Accordingly, the relative crystallinity $X_{(T)}$, at temperature T and cooling rate γ, is given by[30,31]

$$1 - X_{(T)} = \exp[-k_{(T)}/\gamma^n] \tag{4}$$

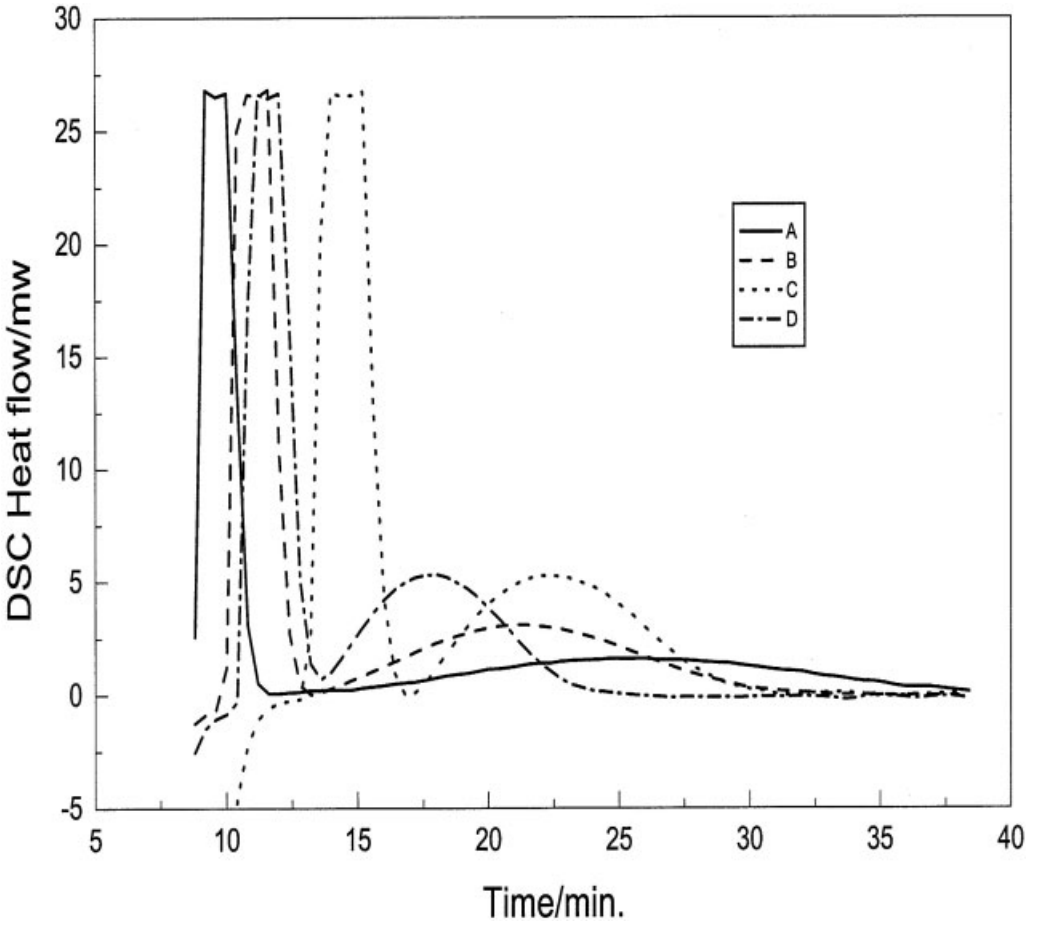

Figure 4 Heat of fusion versus the time for plain iPP and nanocomposites isothermally crystallized at 130°C from the melt: (A) plain, (B) 1 wt % organo-MMT, (C) 2 wt % organo-MMT, and (D) 4 wt % organo-MMT.

where $k_{(T)}$ is the cooling function of nonisothermal crystallization at T and n is the Ozawa index or nonisothermal Avrami exponent. Equation (4) can be linearized as follows:

$$\ln[-\ln(1 - X_{(T)})] = \ln k_{(T)} + n\ln\gamma^{-1} \tag{5}$$

The intercept and slope of $\ln[-\ln(1 - X_{(T)})]$ versus $\ln \gamma^{-1}$ yield $nk_{(T)}$ and n, respectively.

Figure 6 shows the crystallization exotherms for plain iPP and iPP/organo-MMT nanocomposites at a constant cooling rate of −5°C/min. The crystallization of iPP/organo-MMT nanocomposites occurs earlier than that of iPP at higher crystallization temperatures. This indicates that the incorporation of organo-MMT into the iPP matrix increases the crystallization rate of iPP. This finding is in agreement with the previous observation that the incorporation of organo-MMT increases the half-crystallization rate ($1/t_{1/2}$) measured with isothermal crystallization from melts.

Figure 7 shows the DSC exotherms for iPP containing 1 wt % organo-MMT at various cooling rates. The crystallization temperature is lowered as the cooling rate is increased because of thermal lag in DSC.

Figure 8 shows the different degrees of crystallinity of plain iPP and iPP/organo-MMT nanocomposites at various cooling rates. It is obvious from the figure that the degree of crystallinity of all the samples decreases as the cooling rate increases.

The relationship of the heat flow versus the temperature can be used to calculate $X_{(T)}$:[32,33]

$$X_{(T)} = \int_{T_0}^{T}\left(\frac{dH}{dt}\right)dt \Big/ \int_{T_0}^{T_\infty}\left(\frac{dH}{dt}\right)dt \tag{6}$$

TABLE III
Avrami parameters for Plain iPP and iPP/Organo-MMT Nanocomposites Isothermally Crystallized at 130°C from the Melt

	Plain iPP	1 wt % organo-MMT	2 wt % organo-MMT	4 wt % organo-MMT
n'	2.45	2.21	2.19	2.22
$k(s^{-n'}) \times 10^7$	0.19	4.39	20.3	15.2
$t_{1/2}$ (s)	1220	638	336	354

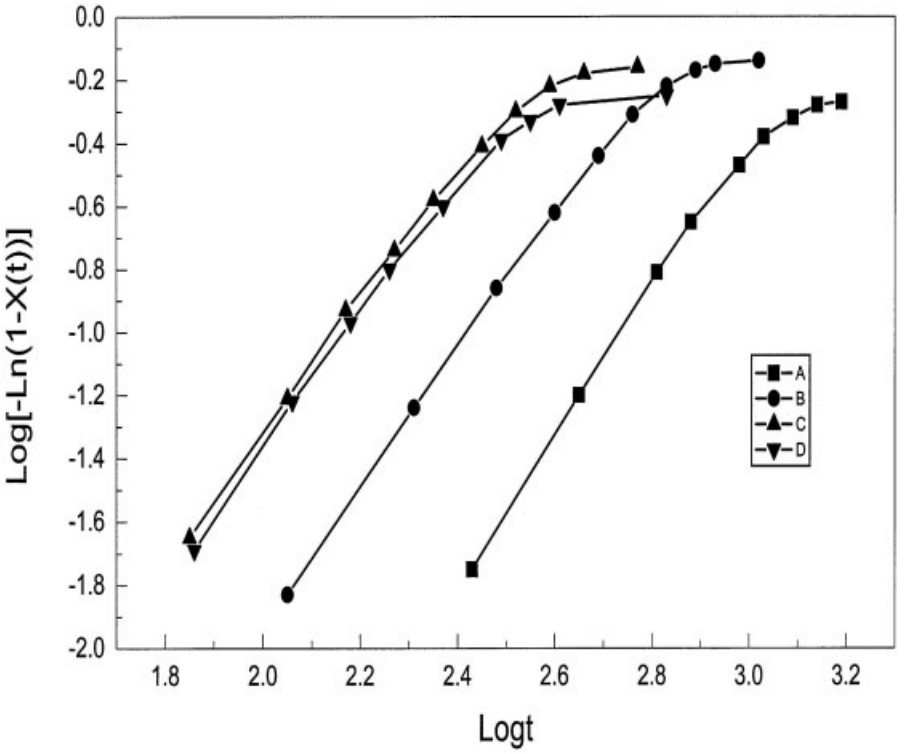

Figure 5 Avrami plots of $\log\{-\ln[1 - X(t)]\}$ versus $\log t$ for plain iPP and nanocomposites: (A) plain, (B) 1 wt % organo-MMT, (C) 2 wt % organo-MMT, and (D) 4 wt % organo-MMT.

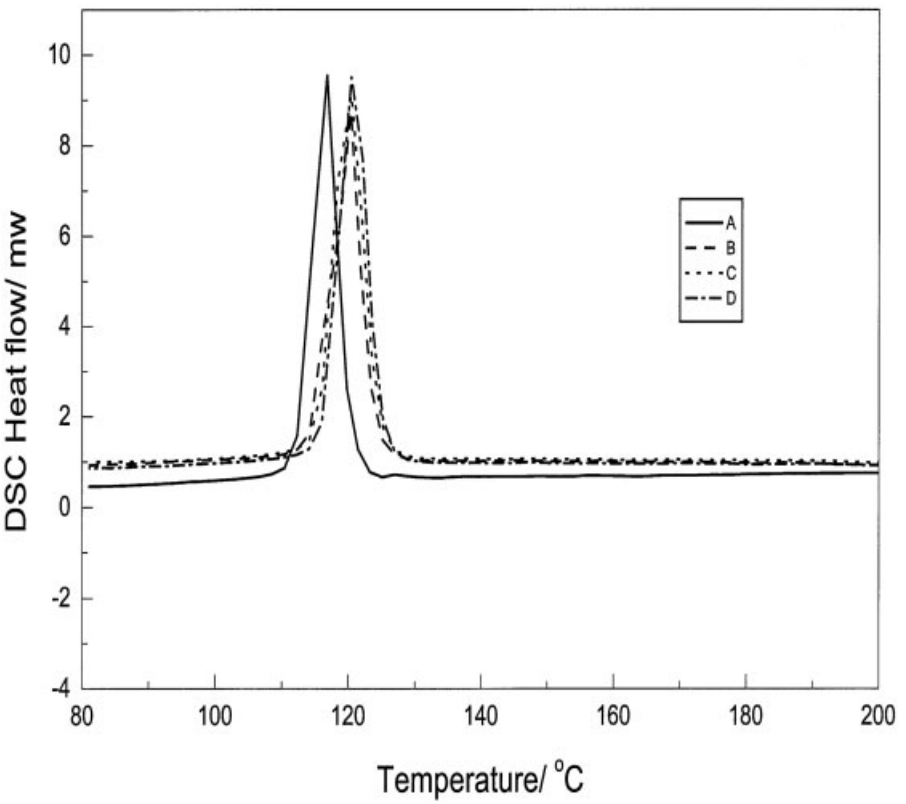

Figure 6 Crystallization exotherms of plain iPP and nanocomposites at a cooling rate of −5°C/min: (A) plain, (B) 1 wt % organo-MMT, (C) 2 wt % organo-MMT, and (D) 4 wt % organo-MMT.

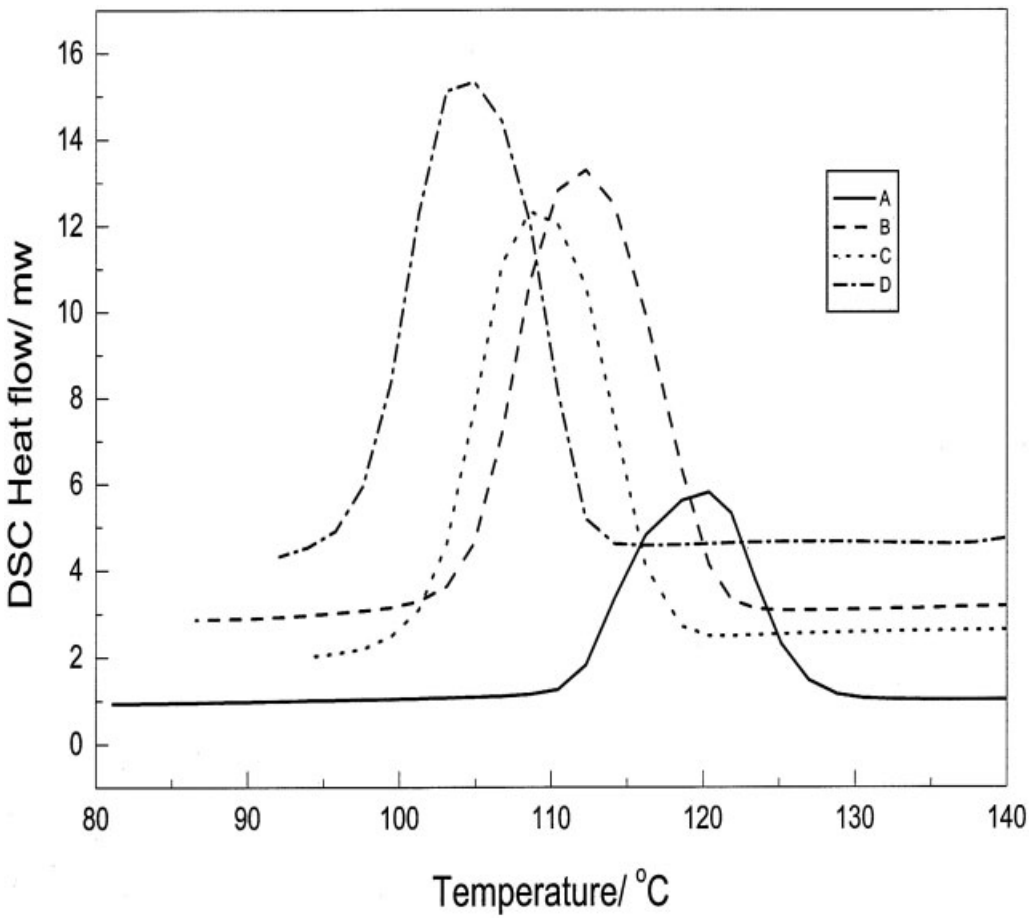

Figure 7 DSC exotherms of iPP containing 1 wt % organo-MMT at various cooling rates: (A) −5, (B) −10, (C) −20, and (D) −25°C/min.

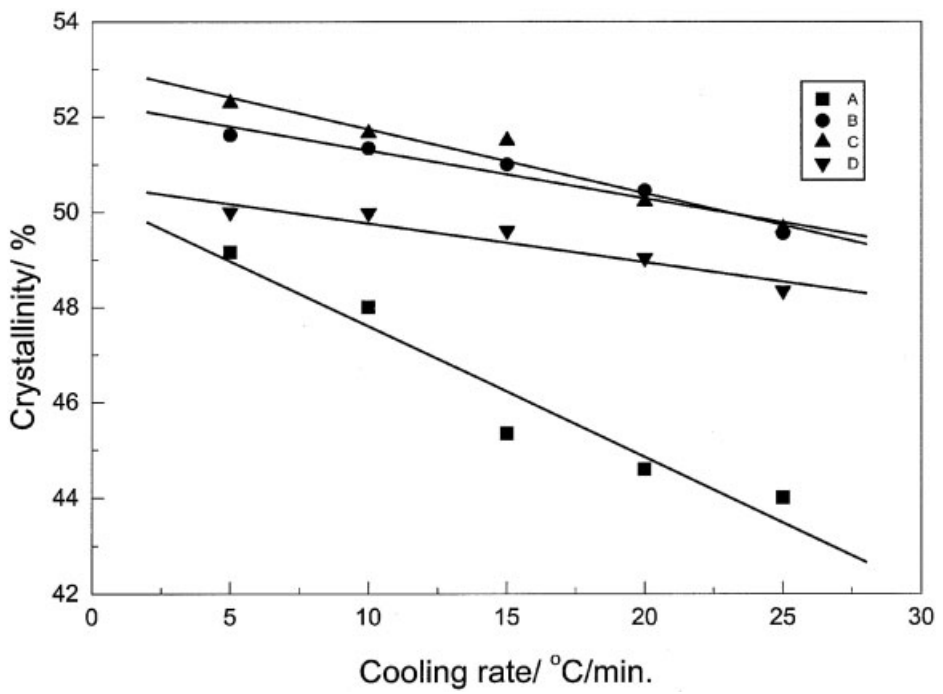

Figure 8 Degree of crystallinity of plain iPP and nanocomposites at various cooling rates: (A) plain, (B) 1 wt % organo-MMT, (C) 2 wt % organo-MMT, and (D) 4 wt % organo-MMT.

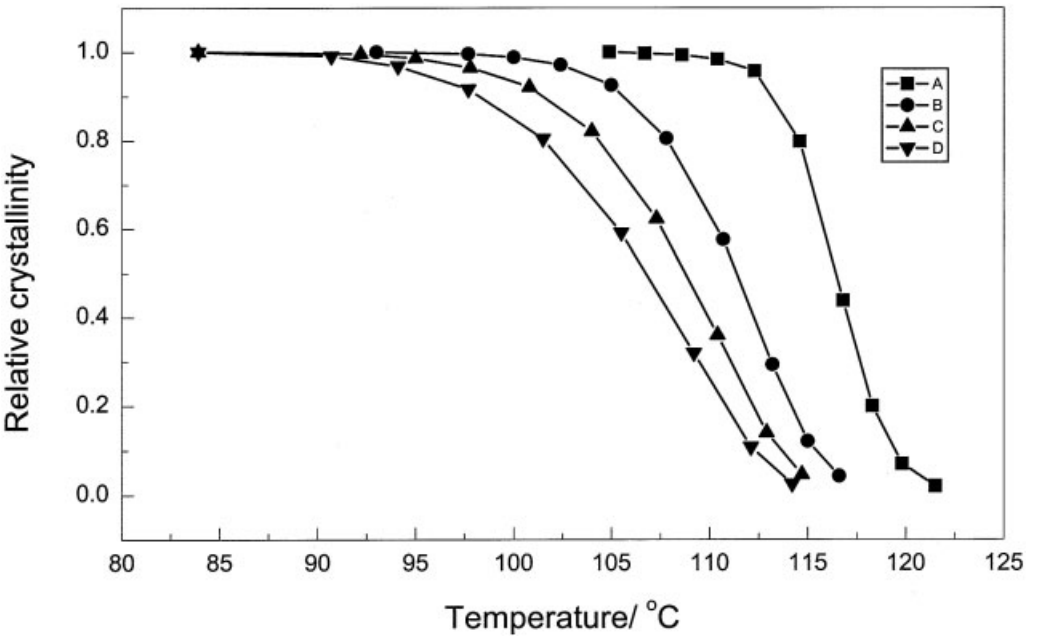

Figure 9 Relative crystallinity of plain iPP versus the temperature at various cooling rates: (A) −5, (B) −10, (C) −15, and (D) −20°C/min.

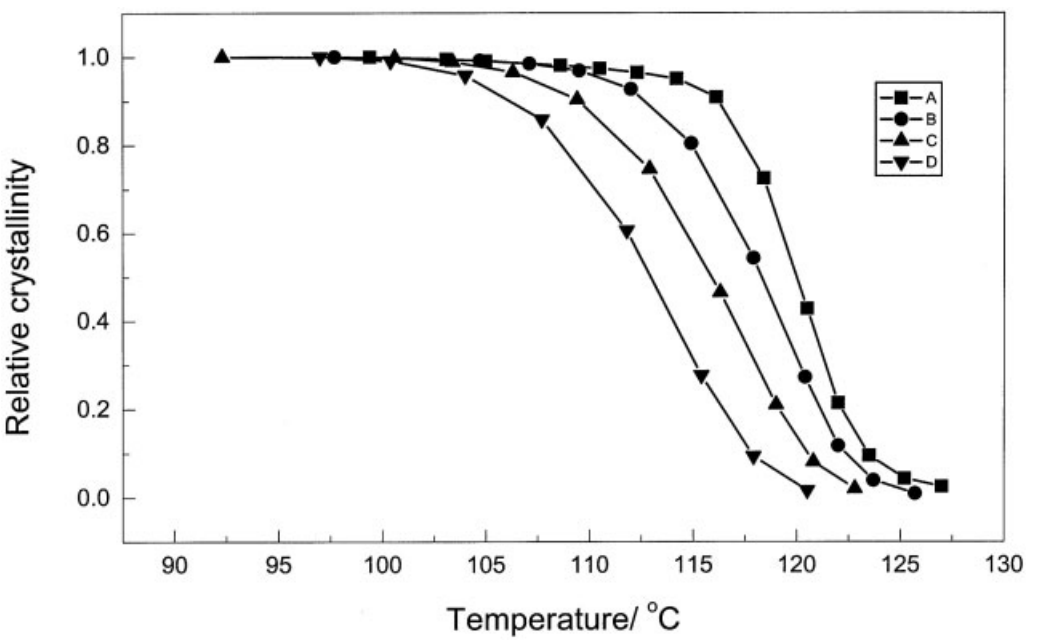

Figure 10 Relative crystallinity of iPP containing 2 wt % organo-MMT versus the temperature at various cooling rates: (A) −5, (B) −10, (C) −15, and (D) −20°C/min.

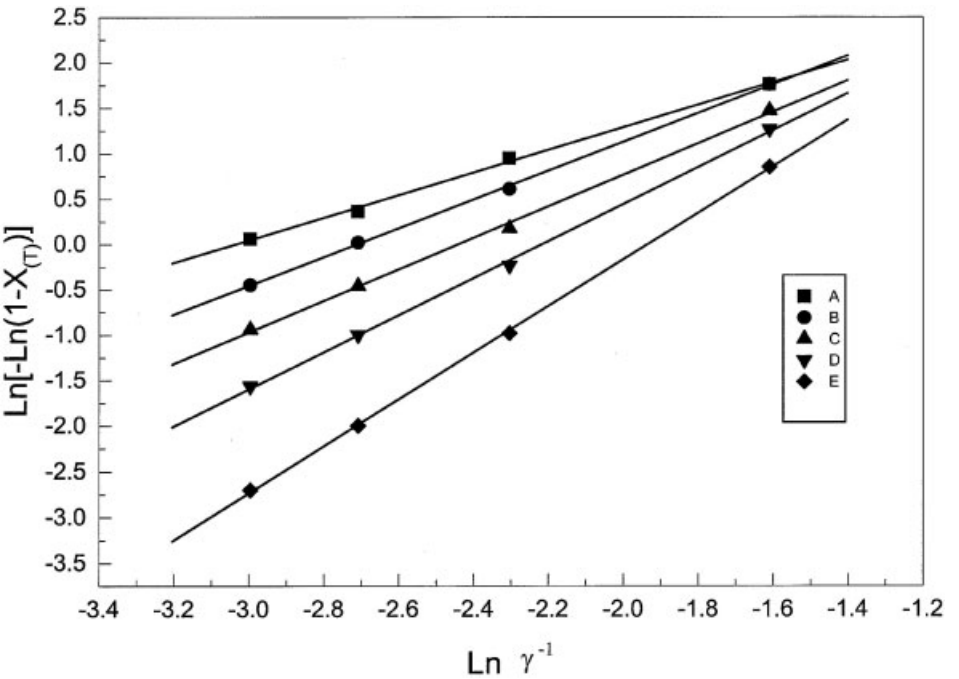

Figure 11 Plots of $\ln[-\ln(1 - X_{(T)})]$ versus $\ln \gamma^{-1}$ for plain iPP at various temperatures: (A) 105, (B) 107, (C) 109, (D) 111, and (E) 113°C.

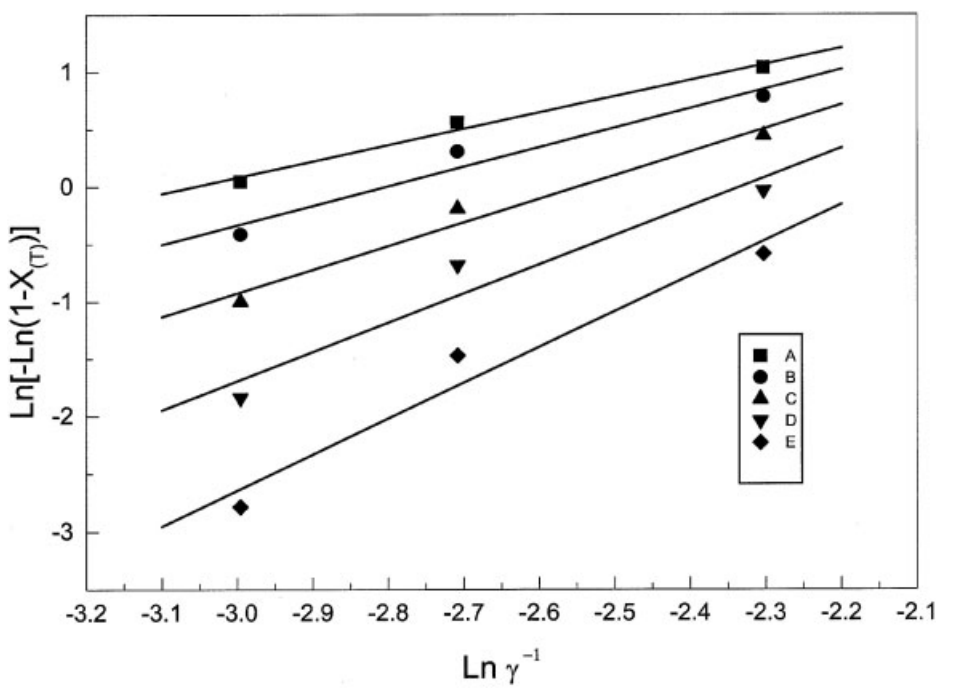

Figure 12 Plots of $\ln[-\ln(1 - X_{(T)})]$ versus $\ln \gamma^{-1}$ for iPP containing 2 wt % organo-MMT at various temperatures: (A) 111, (B) 113, (C) 115, (D) 117, and (E) 119°C.

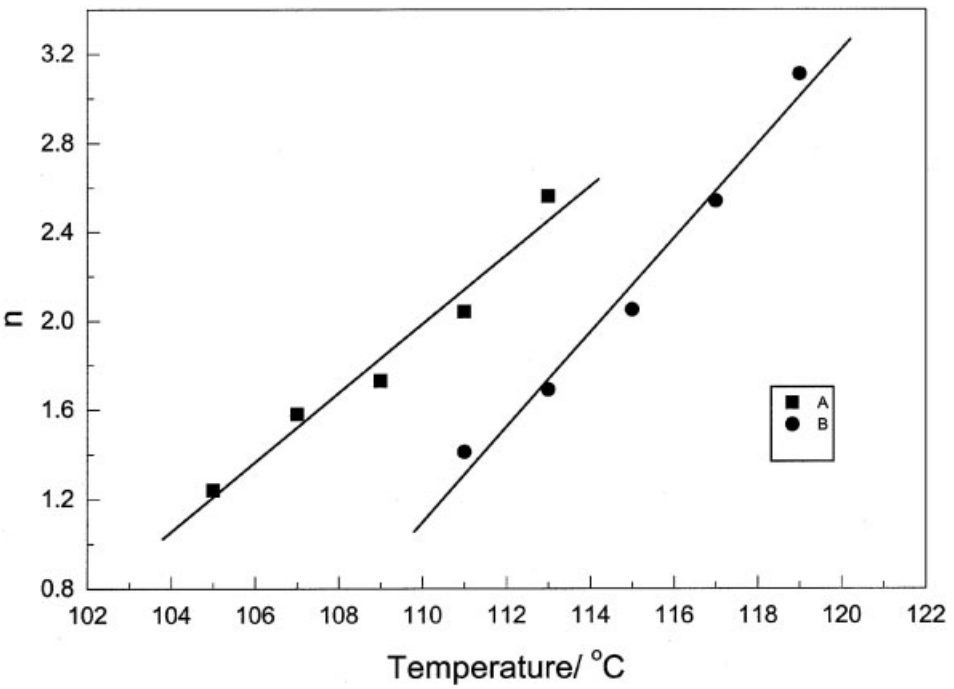

Figure 13 Nonisothermal Avrami exponent (n) versus the temperature: (A) plain and (B) 2 wt % organo-MMT.

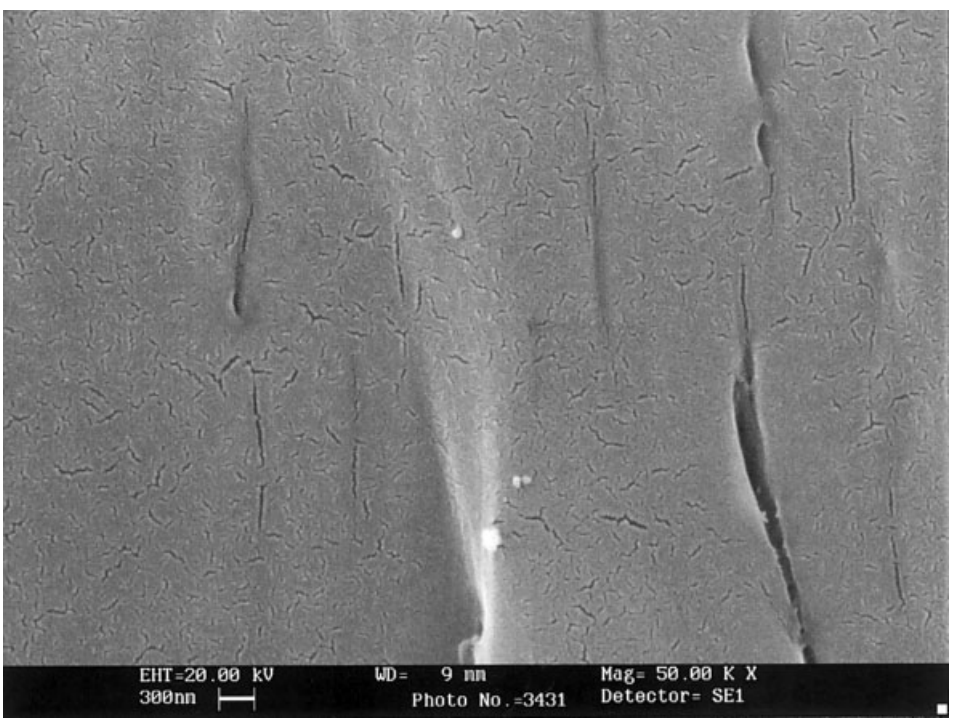

Figure 14 SEM micrograph of the 1 wt % organo-MMT nanocomposite (original magnification, 50,000×). The particles were 100 nm or smaller.

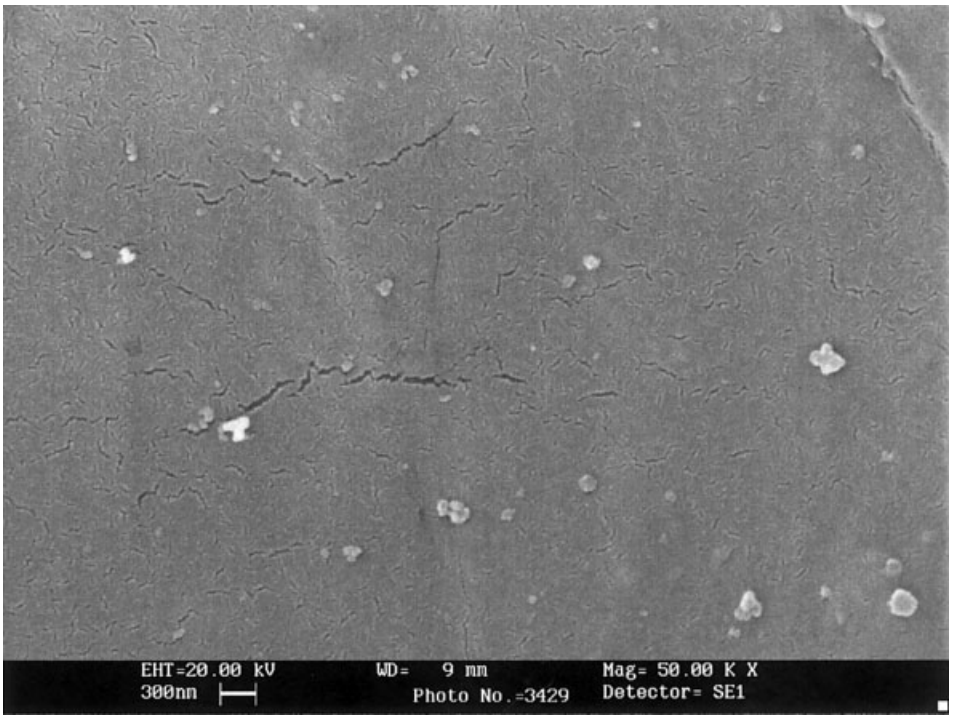

Figure 15 SEM micrograph of the 2 wt % organo-MMT nanocomposite (original magnification, 50,000×).

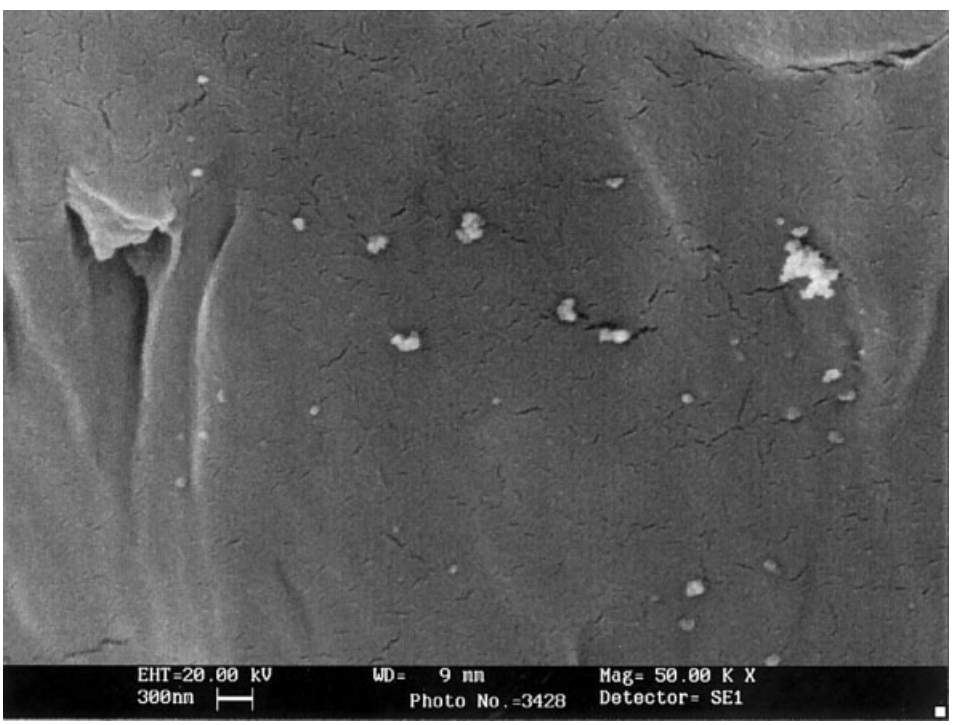

Figure 16 SEM micrograph of the 4 wt % organo-MMT nanocomposite (original magnification, 50,000×).

where T_0 and T_∞ are the lower and upper crystallization temperatures, respectively.

Figures 9 and 10 show the relative crystallinity values of plain iPP and a 2 wt % organo-MMT nanocomposite, respectively, versus the temperature at various cooling rates. The calculated $X_{(T)}$ values have been analyzed according to eq. (5). The left-hand side of eq. (5) has been plotted for a given temperature versus ln γ^{-1}, as illustrated for plain iPP and a 2 wt % organo-MMT nanocomposite in Figures 11 and 12, respectively. The Ozawa equation is applicable to the nonisothermal crystallization of the samples, and the exponent, n, is calculated from the slopes of these straight lines. Figure 13 shows that the nonisothermal Avrami exponent n increases with increasing crystallization temperature. Fractional values of n are common for polymer crystallization.[31] The addition of organo-MMT to iPP reduces n at the same crystallization temperature, and this suggests that the presence of organo-MMT fillers restricts the direction of iPP crystal growth.

SEM

The pellets were cut with a pair of scissors, and the exposed fractured surfaces were examined with SEM. Figures 14–16 show the morphology of iPP containing 1, 2, and 4 wt % organo-MMT. The dispersed organo-MMT particles were 100 nm or smaller. Aggregates were found in the 4 wt % organo-MMT nanocomposite, and this may explain why there is no significant further increase in the crystallization rate relative to that of the 2 wt % organo-MMT nanocomposite.

CONCLUSIONS

The incorporation of organo-MMT fillers into the iPP matrix enhances both the thermal stability and the crystallization rate of iPP and may also change the crystallite growth geometry. Subsequently, the tensile yield strength and modulus both increase, but the elongation at break and the notched Izod impact strength do not change significantly.

The authors acknowledge Jeremy Yeung of the Materials Research Center for the SEM micrographs. The authors also appreciate the helpful suggestions of Si-Dong Li.

References

1. Giannelis, E. P. Adv Mater 1996, 8, 29.
2. Vaia, R. A.; Jandt, K. D.; Kramer, E. J.; Giannelis, E. P. Chem Mater 1996, 8, 2628.
3. Akelah, A.; Salahuddin, N.; Hiltner, A.; Baer, E.; Moet, A. Nanostruct Mater 1994, 4, 965.
4. Vaia, R. A.; Vasudevan, S.; Krawiec, W.; Scanlon, L. G.; Giannelis, E. P. Adv Mater 1995, 7, 154.
5. Krishnamoorti, R.; Vaia, R. A.; Giannelis, E. P. Chem Mater 1996, 8, 1728.
6. Vaia, R. A.; Ishii, H.; Giannelis, E. P. Chem Mater 1993, 5, 1694.
7. Weimer, M. W.; Chen, H.; Giannelis, E. P.; Sogah, D. Y. J Am Chem Soc 1999, 121, 1615.
8. Zeng, C.; Lee, L. J. Macromolecules 2001, 34, 4098.
9. Rong, J.; Li, H.; Jing, Z.; Hong, X.; Sheng, M. J Appl Polym Sci 2001, 82, 1829.
10. Ke, Y.; Long, C.; Qi, Z. J Appl Polym Sci 1999, 71, 1139.
11. Liu, L.; Qi, Z.; Zhu, X. J Appl Polym Sci 1999, 71, 1133.
12. Wang, S.; Long, C.; Wang, X.; Li, Q.; Qi, Z. J Appl Polym Sci 1998, 69, 1557.
13. Liu, X.; Wu, Q.; Polymer 2001, 42, 10013.
14. Qi, Z.; Wang, S.; Zhou, W.; Chin. Pat. CN1247206.
15. (a) Avrami, M. J Chem Phys 1939, 7, 1103; (b) Avrami, M. J Chem Phys 1940, 8, 212.
16. Banks, W.; Gordon, M.; Roe, R. J.; Sharples, A. Polymer 1963, 4, 61.
17. Banks, W.; Sharples, A. Macromol Chem 1963, 59, 233.
18. Eder, M.; Wlochowicz, A. Polymer 1983, 24, 2593.
19. Kozlowski, W. J Polym Sci Part C: Polym Symp 1972, 38, 47.
20. Godovsky, Y. K.; Slonimsky, G. L.; Garbar, N. M. J Polym Sci Part C: Polym Symp 1972, 37, 1.
21. Hillier, I. H. J Polym Sci Part A: Gen Pap 1965, 3, 3067.
22. Lopez, L. C.; Wilkes, G. L. Polymer 1989, 30, 882.
23. Sheldon, R. P. Polymer 1963, 4, 213.
24. Cebe, P.; Hong, S. D. Polymer 1986, 27, 1183.
25. Clark, E. J.; Hoffman, J. D. Macromolecules 1984, 17, 878.
26. Evans, U. R. Trans Faraday Soc 1945, 41, 369.
27. Tobin, M. C. J Polym Sci Polym Phys Ed 1977, 15, 2269.
28. Jeziorny, A. Polymer 1978, 19, 1142.
29. Ziabicki, A. Appl Polym Symp 1967, 6, 1.
30. Ozawa, T. Polymer 1971, 12, 150.
31. Di Lorenzo, M. L.; Silvestre, C. Prog Polym Sci 1999, 24, 917.
32. Pratt, C. F.; Hobbs, S. Y. Polymer 1976, 17, 12.
33. Hammami, A.; Spruiell, J.; Mehrotro, A. K. Polym Eng Sci 1995, 35, 797.